

## Supporting Information for

# Screen printed carbon CsPbBr<sub>3</sub> solar cells with high open-circuit photovoltage

*Isabella Poli,<sup>a b \*</sup> Jenny Baker,<sup>c</sup> James McGettrick,<sup>c</sup> Francesca De Rossi,<sup>c</sup> Salvador Eslava,<sup>d b</sup> Trystan Watson,<sup>c</sup> and Petra J. Cameron<sup>a b \*</sup>*

*<sup>a</sup>Department of Chemistry, University of Bath, Bath BA2 7AY, United Kingdom*

*<sup>b</sup>Centre for Sustainable Chemical Technologies, University of Bath, Bath BA2 7AY, United Kingdom*

*<sup>c</sup>SPECIFIC, Swansea University Bay Campus, Fabian Way, Swansea, SA1 8EN, United Kingdom*

*<sup>d</sup>Department of Chemical Engineering, University of Bath, Bath BA2 7AY, United Kingdom*

## Experimental

All data created during this research are openly available from the University of Bath data archive at <https://doi.org/10.15125/BATH-00530>.

**Device fabrication** The screen printed mesoporous stacks used in this work were fabricated at SPECIFIC, University of Swansea. The perovskite CsPbBr<sub>3</sub> was then infiltrated and cells characterized at University of Bath. Planar devices were fully fabricated in Bath. Both types of cells contained spray pyrolysis titania blocking layers which were deposited using slightly different techniques according to the optimum procedure in each lab.

**EIS theory** Impedance measurements at open circuit at different illumination intensity were carried out on both mC-PSC and C-PSC.

At all intensities three semi-circles were seen in the Nyquist plots. We believe that the impedance response observed at high frequency is associated to the carbon contact ( $C_{hf}$  and  $R_{hf}$ ).  $C_g$  is the geometric capacitance which is voltage-dependent. The parallel resistance that accompanies  $C_g$  is attributed to the recombination resistance  $R_{rec}$ . Previous studies have shown that the chemical capacitance associated to the photogenerated electrons and holes in the perovskite layer is negligible [1].

Recombination is represented by the voltage-dependent recombination resistance  $R_{rec}$ , defined by

$$R_{rec} = \left( \frac{\delta V}{\delta j_{rec}} \right) \quad (1)$$

where,  $J_{rec}$  is the recombination current density. The variation of the  $R_{rec}$  with voltage can be related to the ideality factor  $m$  of the device using

$$\frac{\delta \log R_{rec}}{\delta V} = - \frac{q}{2.303 m k_B T} \quad (2)$$

where  $q$  is the elementary charge,  $k_B$  is the Boltzmann constant and  $T$  is the temperature.

**Optical properties** First, we wanted to check the thermal stability of CsPbBr<sub>3</sub> at 400 °C by measuring the optical properties of a film before and after annealing treatment at 400 °C. Fig. S1(a) shows the UV-Vis absorption spectrum of CsPbBr<sub>3</sub> before and after post-annealing treatment at 400 °C. For comparison, the absorption spectra of MAPbI<sub>3</sub> are also shown. The absorption window of CsPbBr<sub>3</sub> does not change with the annealing treatment, showing high thermal stability. In contrast, MAPbI<sub>3</sub> completely evaporates. CsPbBr<sub>3</sub> has an absorption onset of 530 nm, which corresponds to an energy bandgap of 2.35 eV, as confirmed by the Tauc plot showed in Fig. S1(b).

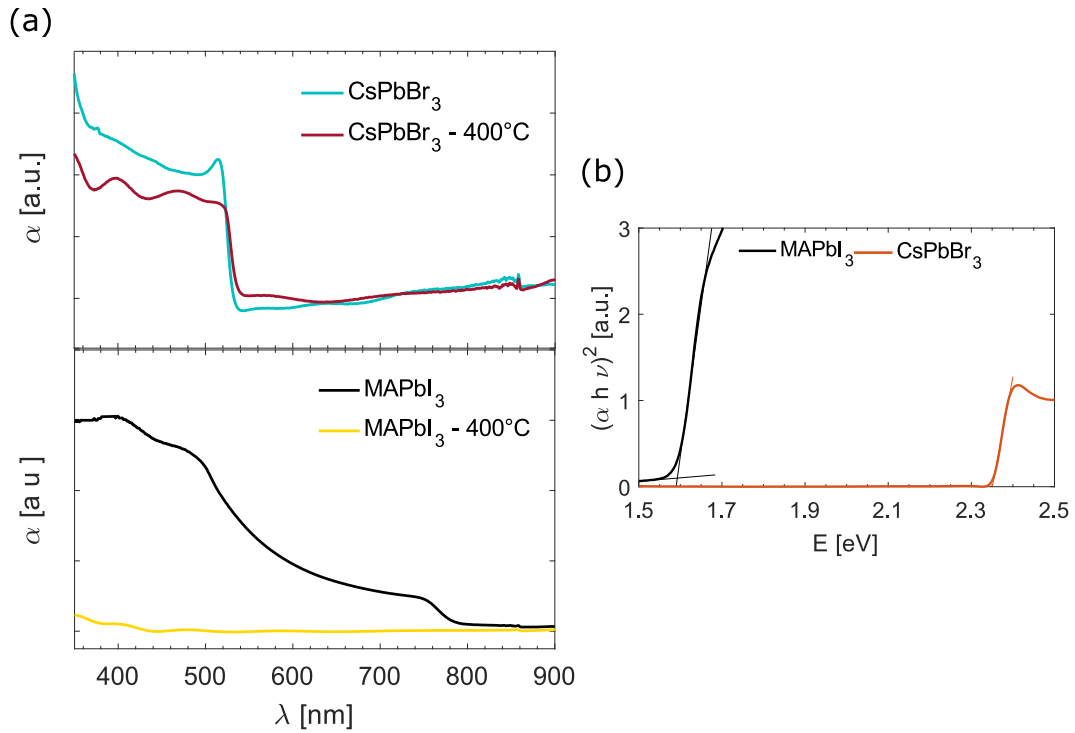


Fig. S1: (a) Absorption spectra of CsPbBr<sub>3</sub> and MAPbI<sub>3</sub> thin films before and after annealing treatment at 400 °C; (b) Tauc plot of MAPbI<sub>3</sub> and CsPbBr<sub>3</sub> films. The energy bandgap values measured through the intercepts with the x is are 1.58 and 2.35 eV respectively

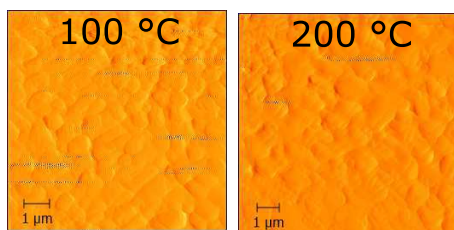


Fig. S2: AFM amplitude images of CsPbBr<sub>3</sub> films annealed at 100 and 200 °C respectively

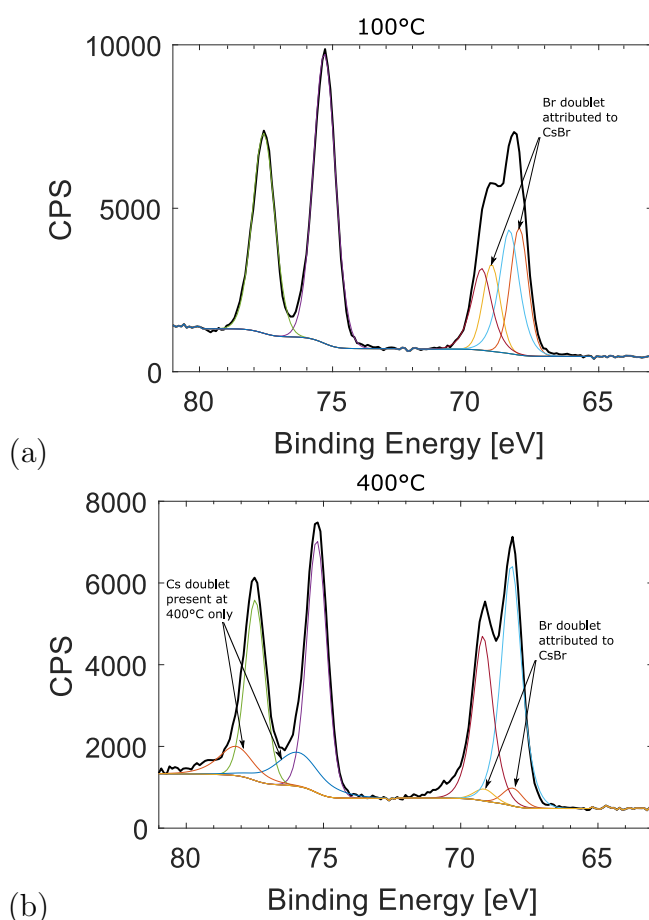


Fig. S3: High resolution XPS spectra of CsPbBr<sub>3</sub> films processed at 100 °C (a) and 400 °C (b) for Cs(4d) and Br(3d). CsBr content decreases with temperature. A higher binding energy component appears on the Cs(4d) spectrum when the film is processed at 400 °C, suggesting that the material is close to the edge of its process window. This extra component is consistent with loss of electron density from the Cs atoms and hence possible oxidation of the material. Notably, the peaks present after annealing at 400 °C are sharper than the ones measured for the film annealed at 100 °C. The sharp peaks indicate less complex chemistry, as the contribution from CsBr to the Br(3d) envelope drops, the FWHM of the Cs(4d<sub>5/2</sub>) peak also drops from 0.97 eV to 0.87 eV, and the FWHM of Pb(4f<sub>7/2</sub>) peak also drops from 1.00 to 0.81 eV

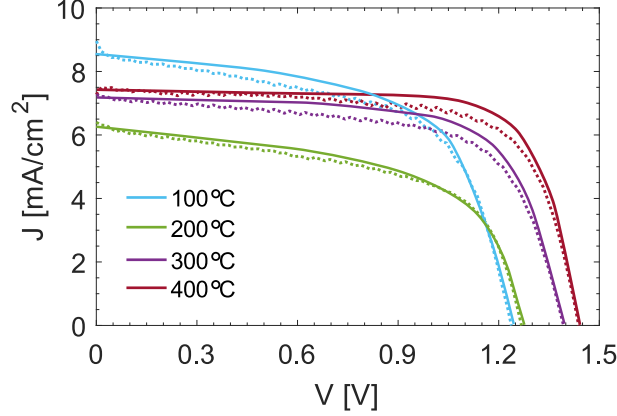


Fig. S4: JV curves of 4 different mC-PSC fabricated in the same batch and each one post-annealed at a different temperature (100, 200, 300 and 400 °C)

**JV curves m-PSC** JV curves of an average performing mC-PSC are shown in Fig. S5(a). The main PV parameters and the curves measured under forward scan are shown in Table S1 and Fig. S6. The same device was systematically annealed at 100, 200, 300 and 400 °C and tested after each temperature. Four different batches were measured following this procedure. This experiment allowed us to monitor the variation of main PV parameters on the same device as a function of the post-annealing temperature. The PV parameters that mainly change with temperature are the open circuit voltage and the fill factor. The  $V_{oc}$  trend with temperature is shown in Fig. S5(b). Box plots of the other PV parameters are shown in Fig. S7. The  $V_{oc}$  increases with annealing temperature, while the FF drops-off. Voltage and fill factor compensate each other and the PCE does not change considerably with annealing temperature.

Table S1: Average PV parameters for  $CsPbBr_3$  mC-PSC showed in Fig. S6

Parameter	100	200	300	400
$J_{sc}$ [mA/cm <sup>2</sup> ]	6.78	6.73	6.58	6.67
$V_{oc}$ [V]	1.21	1.24	1.29	1.35
FF [-]	55.14	59.31	52.79	48.29
PCE [%]	4.53	4.96	4.47	4.35

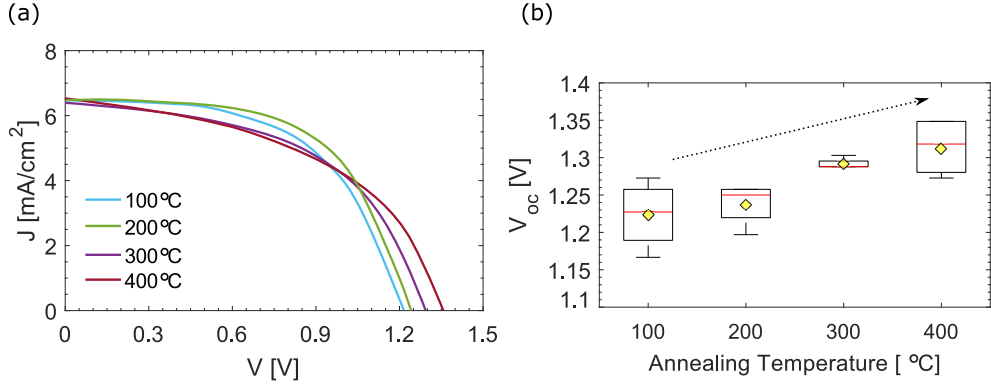


Fig. S5: (a) JV curves of an average performing mC-PCS post annealed at different temperatures; The device with the highest open circuit voltage was post-annealed at 400 °C and exhibited  $V_{oc}=1.35$  V,  $J_{sc}=7.7$  mA cm<sup>-2</sup>, FF=50.5 and PCE=5.2%. The most efficient cell was annealed at 200 °C and exhibited  $V_{oc}=1.26$  V,  $J_{sc}=7.6$  mA cm<sup>-2</sup>, FF=58.7 and PCE=5.6%. (b) Box-plots of  $V_{oc}$  of mC-PSC annealed at different temperatures

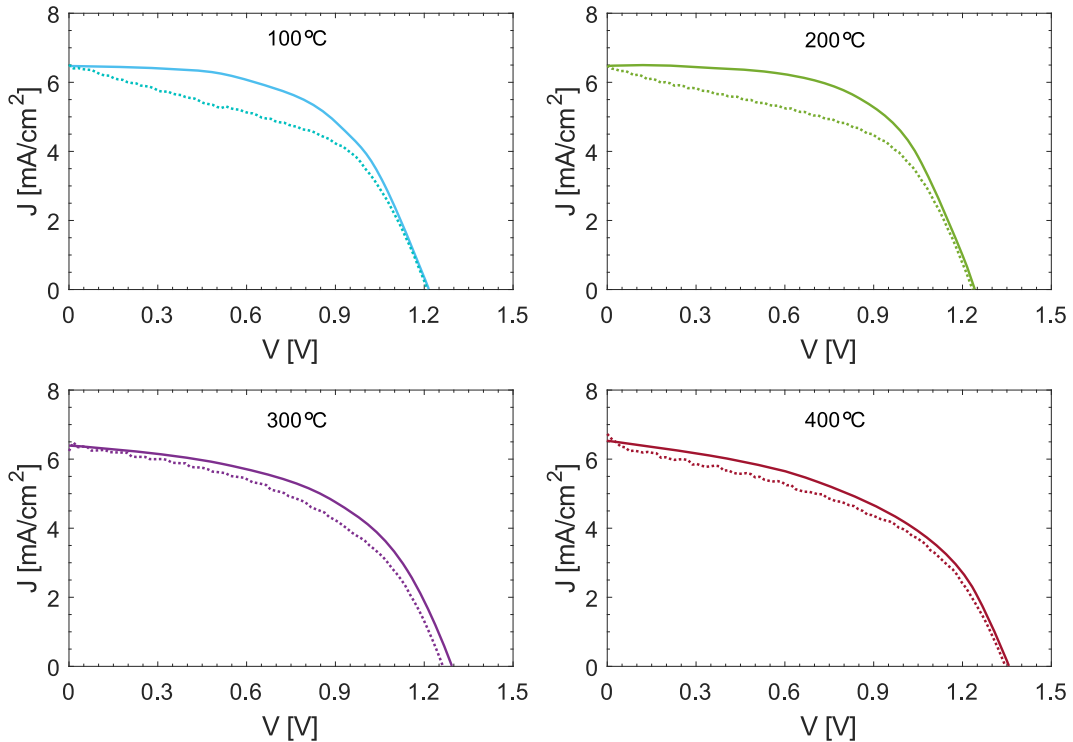


Fig. S6: Forward and reverse scans of a mC-PSC systematically processed at different temperatures (JV curves measured after each annealing step)

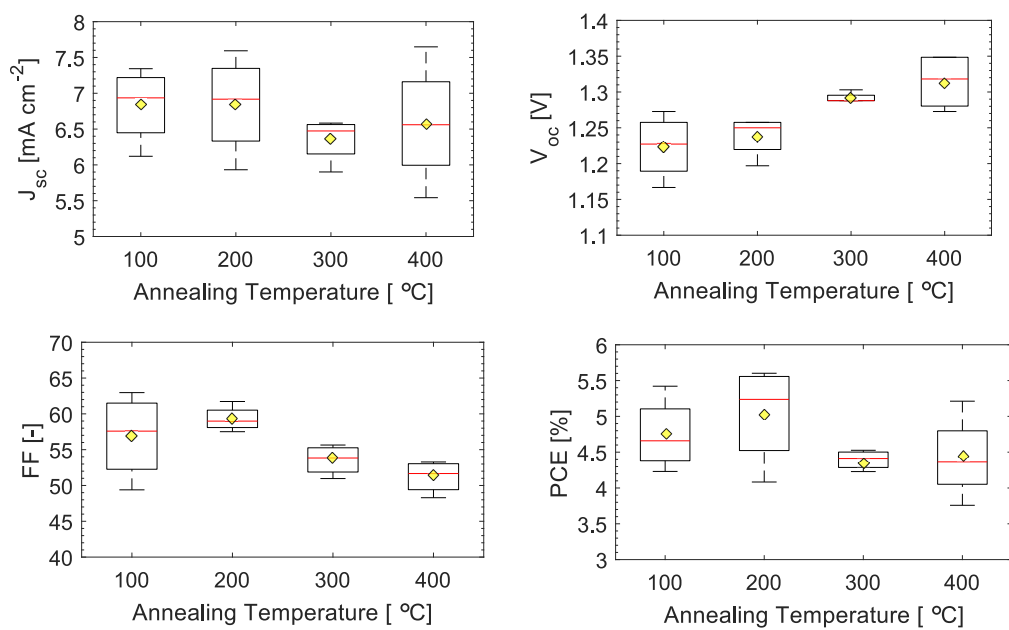


Fig. S7: Box plots of main photovoltaic parameters of mC-PSC. Each cell was systematically annealed at 100, 200, 300 and 400 °C and measured after each temperature

**EQE of mC-PSC** Very little changes in photocurrent were observed with post-annealing temperature. This results is further confirmed by the external quantum efficiency (EQE) measurements shown in Fig. S8. The integrated photocurrent of samples processed at different temperatures does not considerably change and very similar short circuit current values are achieved. The EQE spectrum of the sample processed at 400 °C shows lower intensities at 300-350 nm. This can be related to partly oxidation of the CsPbBr<sub>3</sub> material due to fast heating that might have damaged the mesoscopic layers TiO<sub>2</sub> and ZrO<sub>2</sub>.

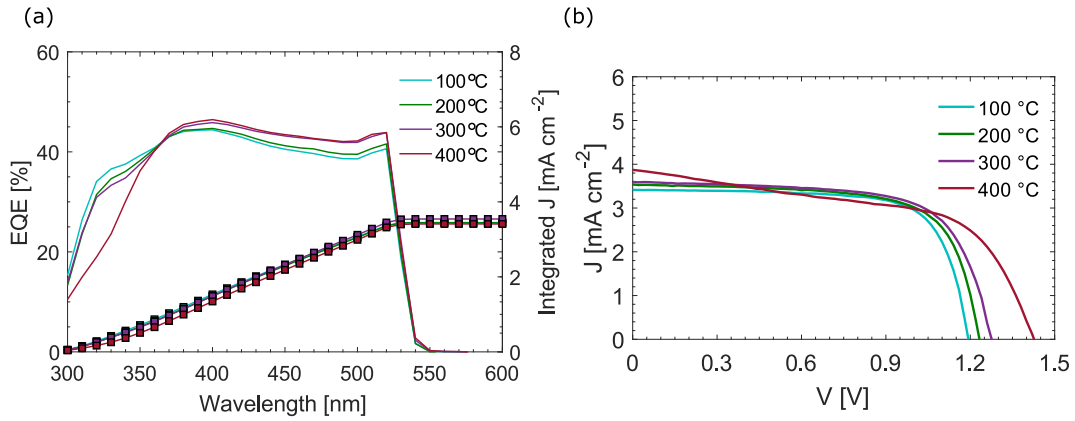


Fig. S8: (a) EQE spectra and integrated current of 4 different mC-PSC devices post-annealed at different temperature after fabrication; (b) JV curves of the mC-PSC devices tested for EQE spectra acquisition

**mC-PSC annealed at 350 °C** XPS analysis showed that when processing CsPbBr<sub>3</sub> films at 400 °C, sometimes oxidation of the material occurred, indicating that the material is close to the edge of its processing window. This phenomenon may be more or less pronounced due to small changes in the annealing temperature and heating and cooling time which may lead to more evident losses in the FF. When processed at an intermediate temperature between 300 and 400 °C, such as 350 °C, the infiltrated CsPbBr<sub>3</sub> remains homogeneously yellow through the carbon layer and no sign of clear oxidation is observed. Fig. S9 shows the (a) JV curve of a mC-PSC post-annealed at 350 °C and the (b) stabilised power output measurement over 60 s. The cell was biased to the maximum power point voltage determined by the JV sweep, which is 1.11 V.

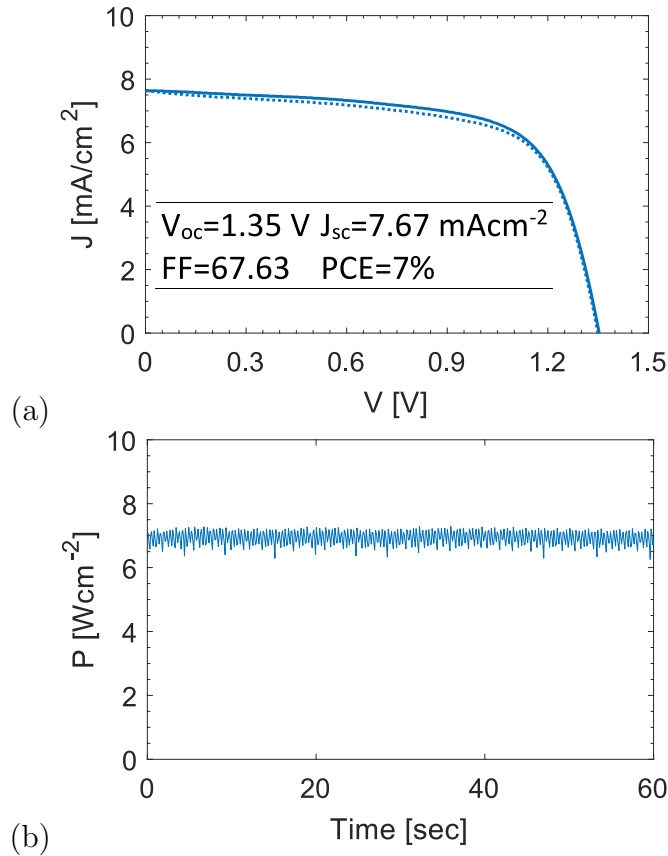


Fig. S9: (a) JV curve of a mC-PSC post-annealed at 350 °C; (b) Stabilised power output measurement over 60 s

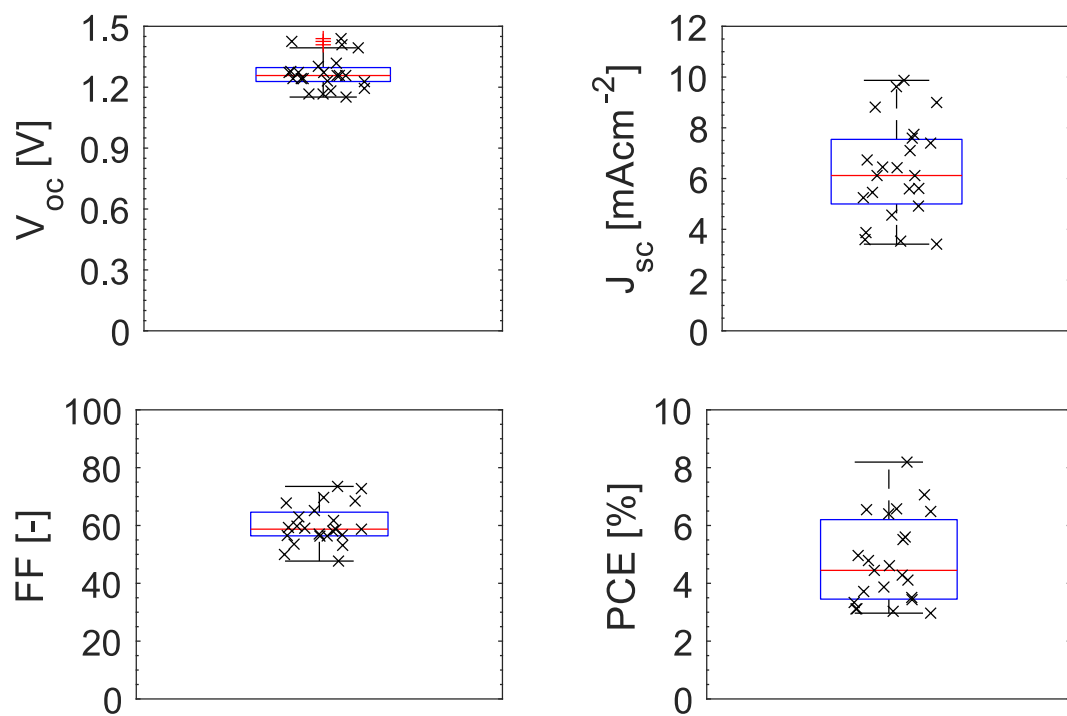


Fig. S10: Box plots of main photovoltaic parameters of mC-PSC post-annealed at 400 °C. Over 20 devices fabricated in different batches were measured

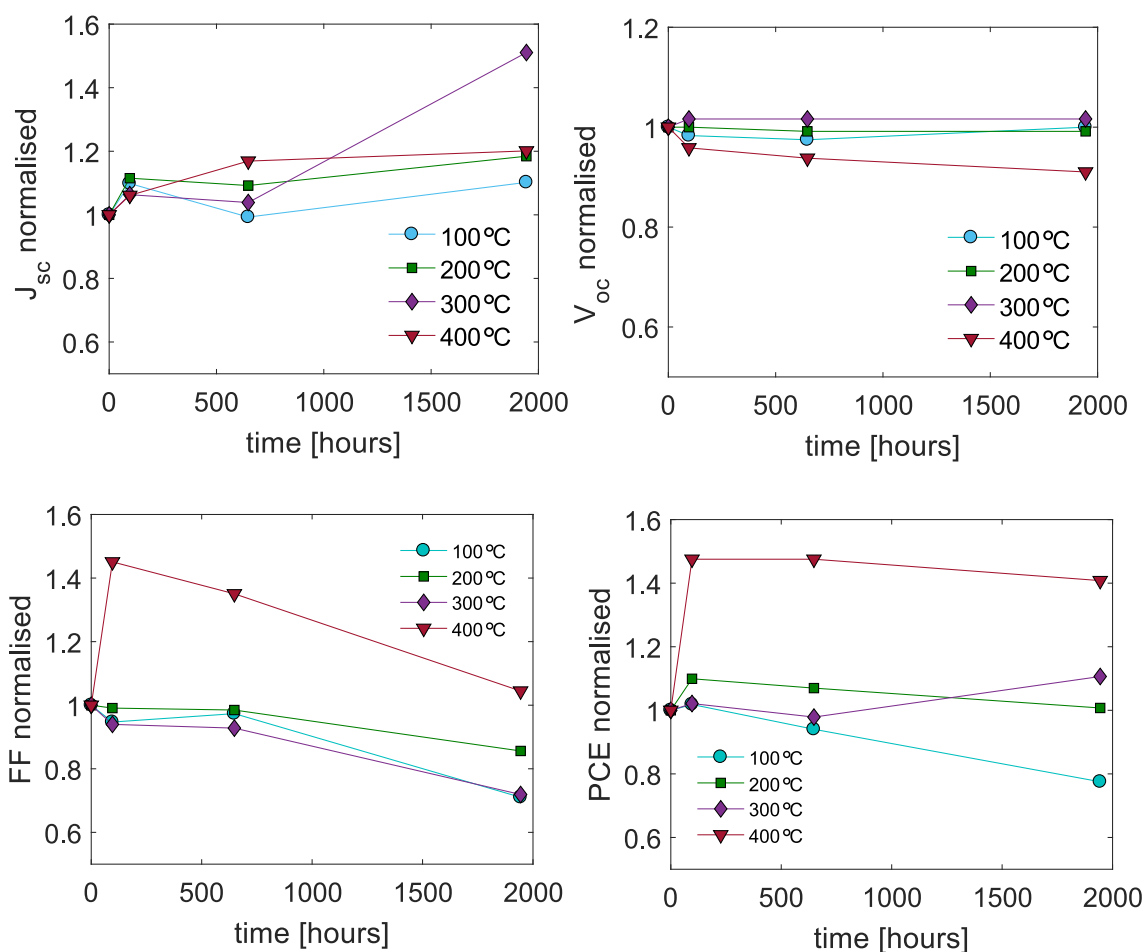


Fig. S11: Variation of the main photovoltaic parameters of mC-PSC annealed at different temperatures overtime. During this time the cells were left in an ambient atmosphere without encapsulation, in the dark, at open circuit (also known as shelf-stability)

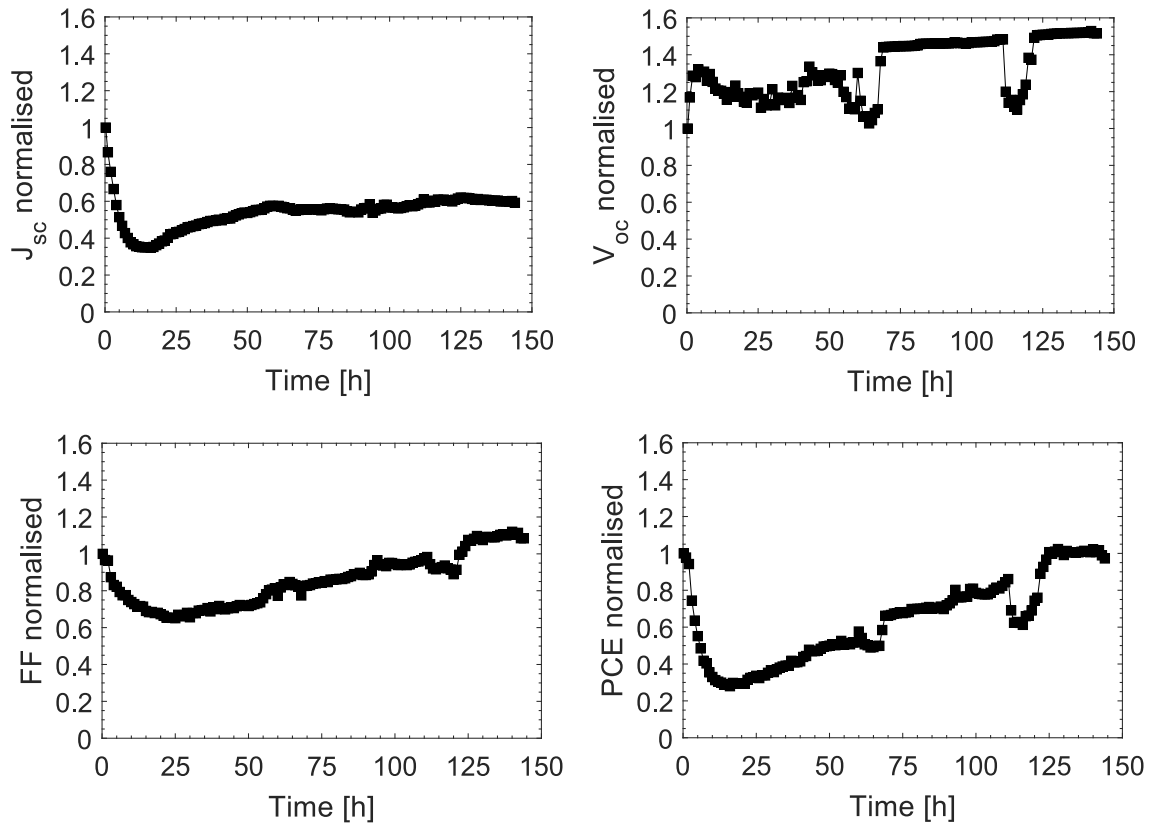


Fig. S12: Variation of the main photovoltaic parameters of a mC-PSC overtime. During this time the unencapsulated cell was monitored under continuous illumination, at short circuit conditions and HR of 50 %

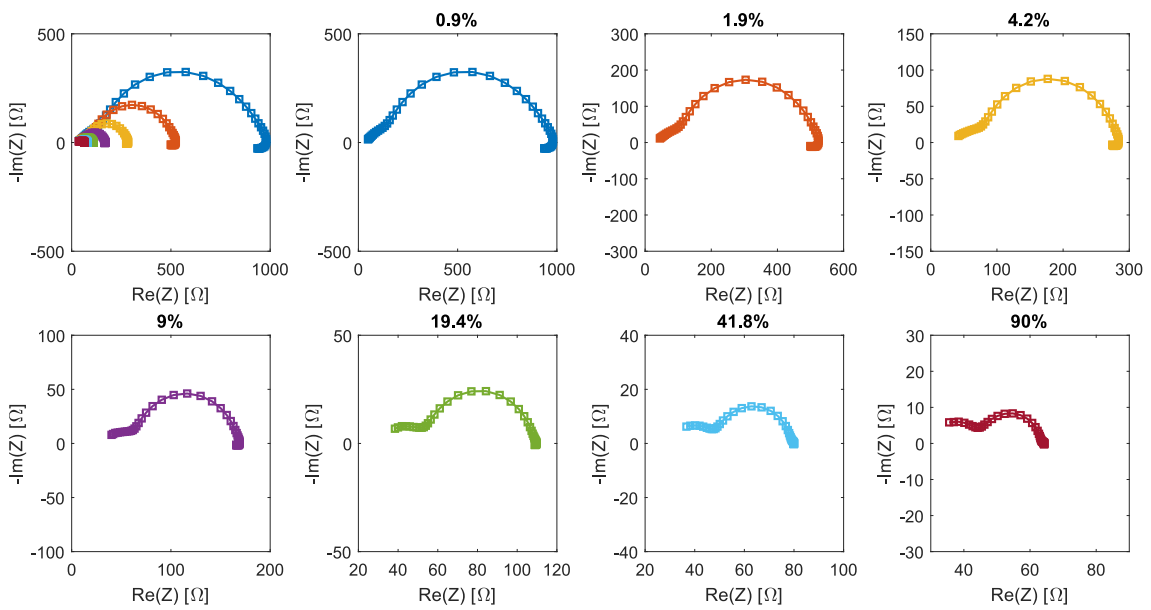


Fig. S13: Nyquist plots measured at open circuit under different illumination intensities for a mC-PSC device post-annealed at 100 °C

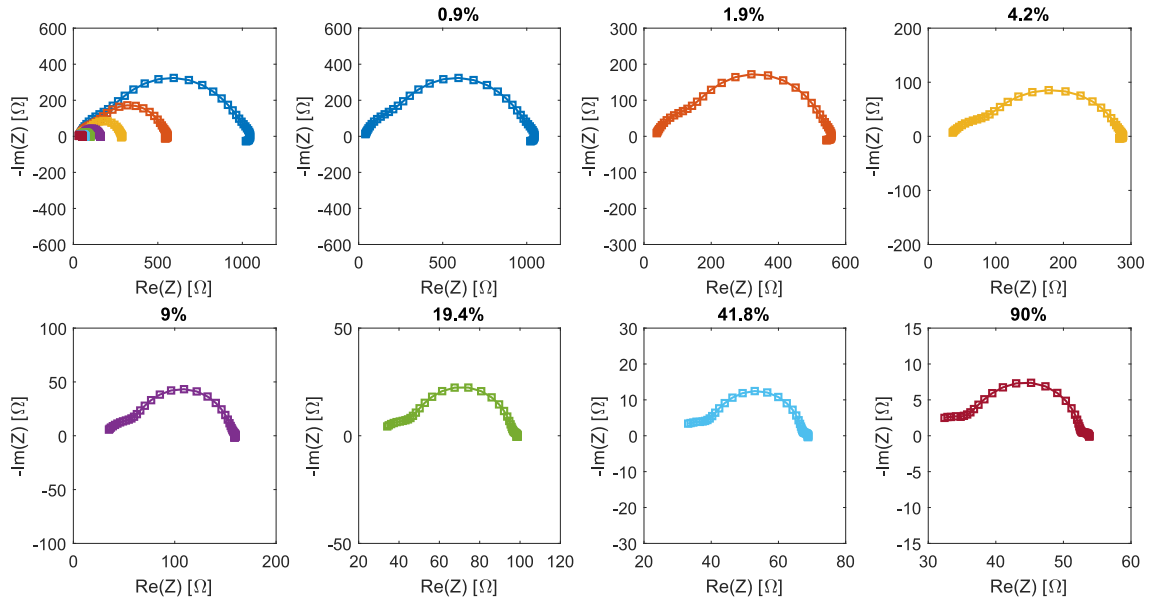


Fig. S14: Nyquist plots measured at open circuit under different illumination intensities for a mC-PSC device post-annealed at 200 °C

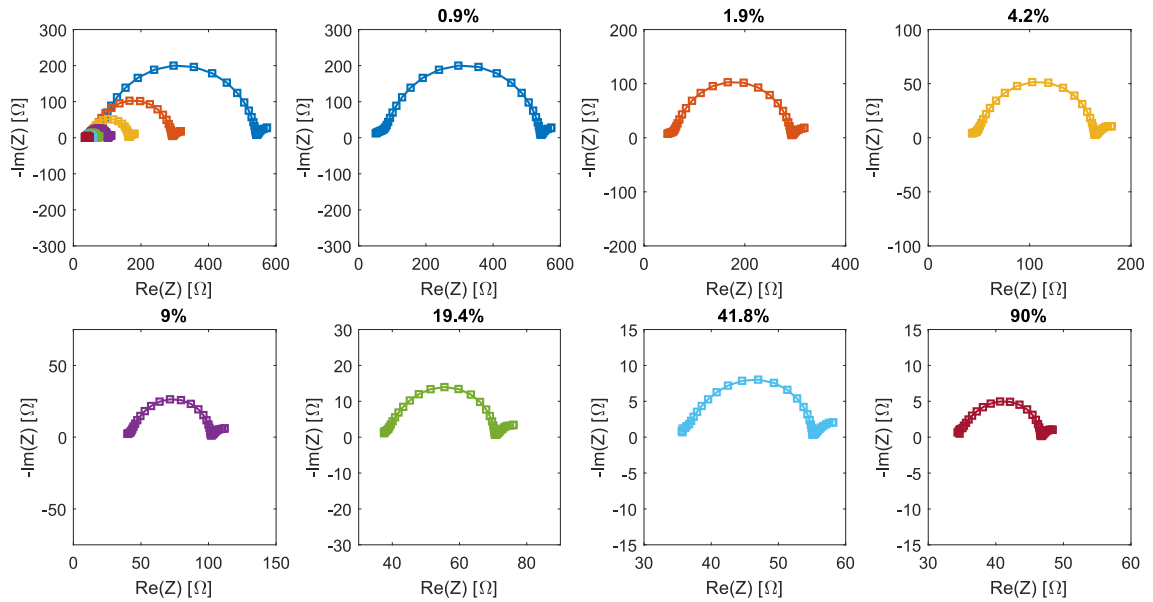


Fig. S15: Nyquist plots measured at open circuit under different illumination intensities for a mC-PSC device post-annealed at 300 °C

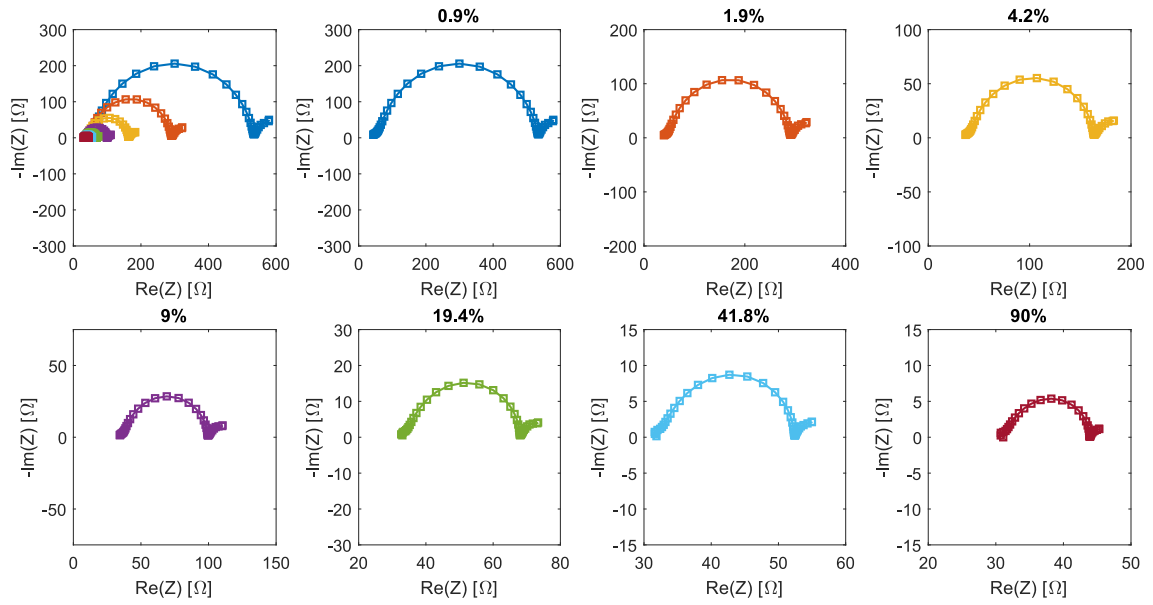


Fig. S16: Nyquist plots measured at open circuit under different illumination intensities for a mC-PSC device post-annealed at 400 °C

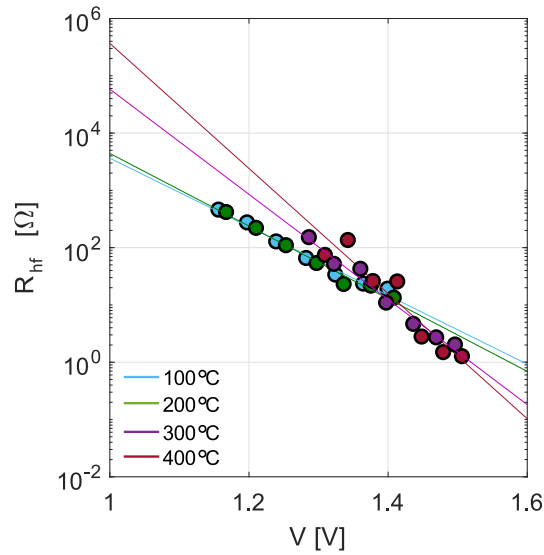


Fig. S17: High frequency recombination obtained by fitting the HF semicircle of EIS measured at open circuit at different illumination intensities of mC-PSC post-annealed at different temperatures

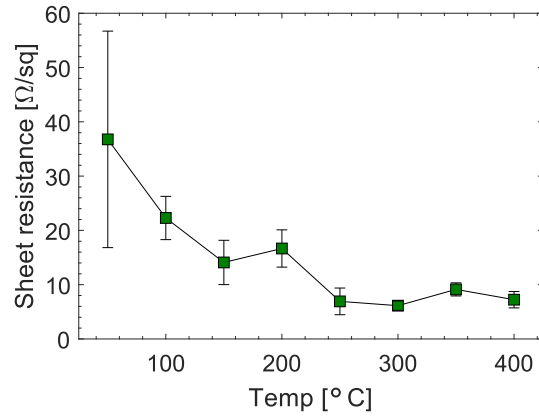


Fig. S18: Sheet resistance of a film of carbon paste measured with a 4-point probe. The resistance was measured after annealing the carbon film at different temperatures

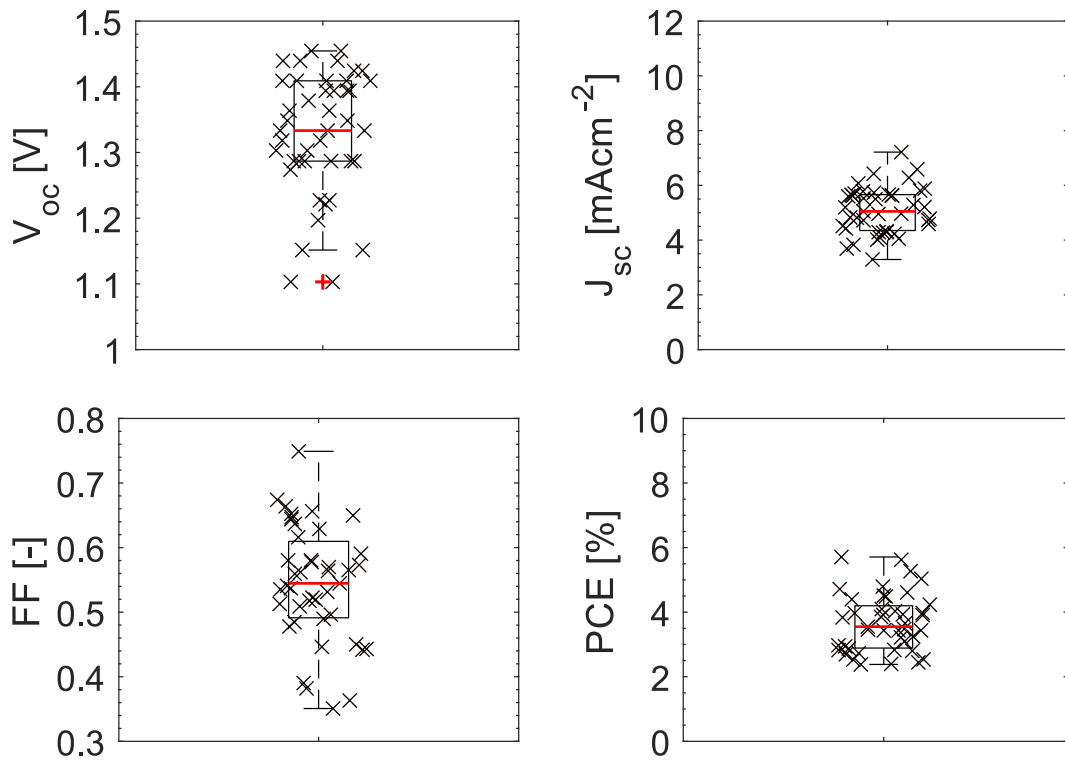


Fig. S19: Box plots of main photovoltaic parameters of C-PSC annealed at 400 °C. Over 40 devices were fabricated in different batches and measured in different days

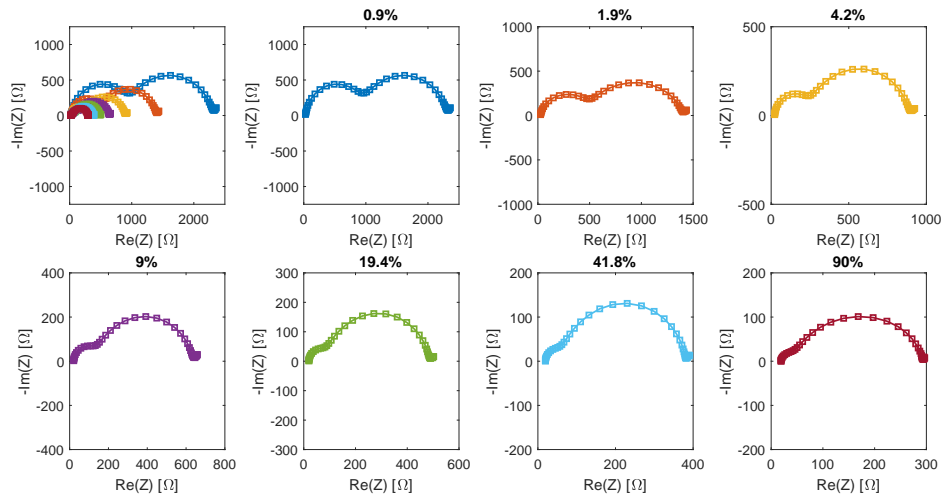


Fig. S20: Nyquist plots measured at open circuit under different illumination intensities for a C-PSC device post-annealed at 400 °C

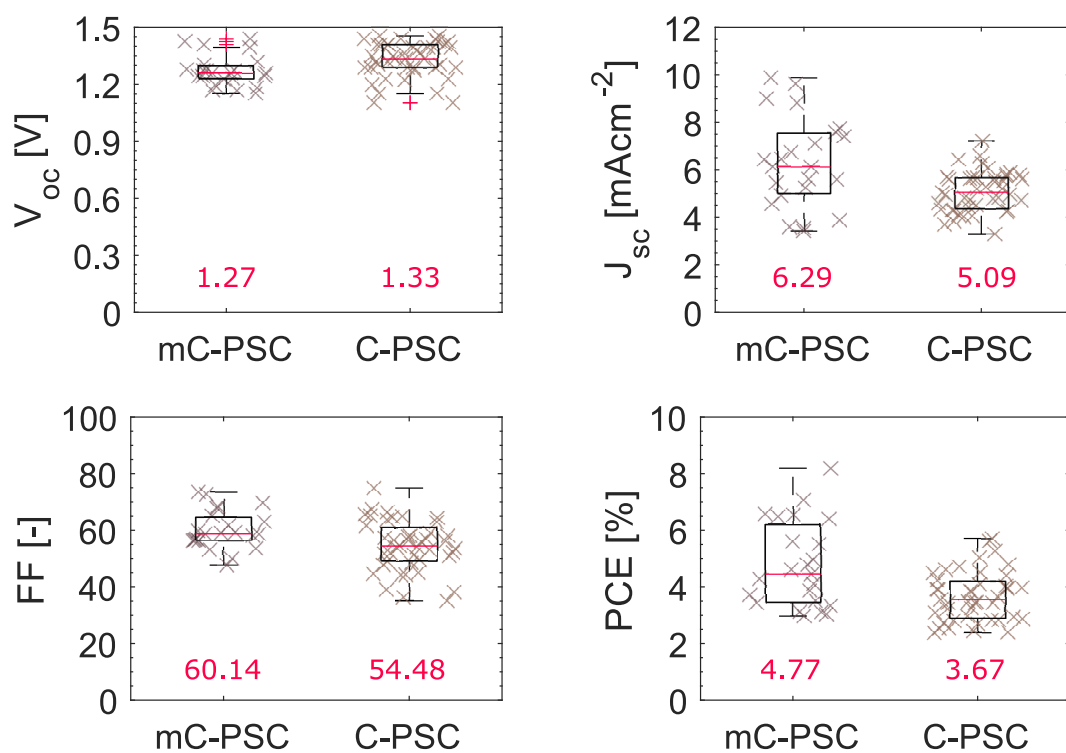


Fig. S21: Box plots of the main PV parameters measured for mC-PSC and C-PSC processed at 400°C. All devices have been measured under 1 sun with active area of 0.25 cm<sup>2</sup>

# Bibliography

- [1] A. Pockett, G. E. Eperon, T. Peltola, H. J. Snaith, A. B. Walker, L. M. Peter, and P. J. Cameron, “Characterization of Planar Lead Halide Perovskite Solar Cells by Impedance Spectroscopy, Open Circuit Photovoltage Decay and Intensity-Modulated Photovoltage/Photocurrent Spectroscopy,” *The Journal of Physical Chemistry C*, vol. 119, no. 7, pp. 3456–3465, 2015.